Hindawi Publishing Corporation
Journal of Materials
Volume 2013, Article ID 597616, 9 pages
http://dx.doi.org/10.1155/2013/597616

Research Article

RTV Silicone Membranes as Agents to Confine the Liquid Components in Dye Sensitized Solar Cells

Antonino Bartolotta, Giuseppe Calogero, Cristina Crupi, and Gaetano Di Marco

CNR-IPCF, Consiglio Nazionale delle Ricerche—Istituto per i Processi Chimico-Fisici, Sede di Messina, Viale Ferdinando Stagno d'Alcontres, No. 37, 98158 Messina, Italy

Correspondence should be addressed to Antonino Bartolotta; bartolotta@me.cnr.it

Received 30 April 2013; Accepted 2 October 2013

Academic Editor: Antoni Morawski

Selected silicone membranes are investigated in order to find attractive multifunctional materials as liquid confining flexible agents with good heat resistance as well as low affinity towards the chemical specimens commonly used in dye sensitized solar cells (DSSC). In fact, the leakage and/or volatilization of liquid components inside DSSC remains one of the most critical obstacles in the progress of this technology from laboratory scale to large area applications. Dynamic mechanical spectroscopic, differential scanning calorimetric, and thermogravimetric analyses on dry membranes were performed in order to investigate their mechanical properties and their thermal stability. By a further comparative study between the equilibrium uptake and the adsorption-desorption process of a nitrile based solution, useful indications about the ability of these networks to encapsulate the liquid mixture were inferred. Moreover, a rough evaluation of porosity was also carried out, giving results which are in agreement with surface morphology observed by scanning electron microscopy and atomic force microscopy. In the light of the results obtained by the different experimental techniques the confinement capability of these membranes towards the liquid components inside a DSSC is discussed.

1. Introduction

In the last few decades, DSSCs have attracted the interest of many academic and industrial communities as powerful and promising devices for the conversion of solar energy in electricity at low cost and low environmental impact [1–6]. At present, the highest photovoltaic efficiency has been reported for DSSCs based on liquid electrolyte solution [2] which, typically, consists of a redox couple dissolved in organic solvent. Unfortunately, the use of liquid components has some disadvantages due to their leakage and volatilization at elevated temperatures [7, 8]. This is a technological problem which could be sorted out by using suitable sealing materials without introducing substances that can harm the cell long-term stability. Furthermore, high repeatability of the laboratory tests, obtained by different research teams, is essential in order to transfer the experimental progresses in outdoor applications. In this context, an essential criterion for reliable comparative tests is a high reproducibility in the manufacture of the laboratory cell prototypes, usually assembled and clipped in an open sandwich-type arrangement [5]. Many sealing materials have been suggested in order to confine the liquid electrolyte inside the DSSCs. Hot-melt ionomeric resins and materials based on melting glass frits have been employed as sealing agents [9, 10]. Nevertheless, the use of these materials introduces further drawbacks such as the solvent and moisture absorption under thermal stress [9] as well as the poisoning of the Pt-catalyst at the cell counterelectrode [10]. Moreover, with these specimens, the cell edges are permanently sealed so that the specific composition of the single components as well as the cell arrangement cannot be changed and the prototype remains useless for further laboratory tests. In this context, we believe that the use of elastomeric networks as removable frame, with properties tailored to the stringent standard performances required in the DSSCs (i.e., elevate temperatures, hostile chemical environments, etc.), could be a satisfactory sealing strategy for the laboratory routine.

In this manner, different tests would be possible on the same cell by varying type, concentration, and/or composition of the individual components maintaining unchanged the geometrical arrangement.

Among elastomeric materials currently available, silicone networks represent a special class of polymers which have been widely applied to various industrial and consumer products. Their unique characteristics such as high thermal stability, excellent mechanical and chemical resistance, waterproof, low toxicity, and sealing capability derive from the presence of silicon oxide fragments in the silicone network [11, 12].

This work focuses on the mechanical properties, thermal stability, and surface morphology of three membranes obtained by commercial room temperature vulcanizing (RTV) silicone rubbers which are expected to display most of the desirable solvent resistance required in the manufacture of these devices. Dynamic mechanical spectroscopy (DMS) measurements were carried out in dry and wet membranes in order to investigate the influence of the liquid components in the temperature region around the glass-rubber transition. The thermal behaviour of dry silicone membranes (SMs) was investigated by performing thermogravimetric (TG) and differential scanning calorimetric (DSC) experiments. The TG results on solvent saturated samples were compared with liquid uptake data and a relationship between the solvent desorption and the confinement characteristics of the selected membranes towards the liquid components was found.

Finally, SMs were analyzed by scanning electron microscopy (SEM) and atomic force microscopy (AFM) in order to investigate their surface morphology which strongly influences the absorption-desorption properties of the membranes. The microscopic analysis revealed different surface morphologies which were in agreement with both the experimental density and porosity values.

The encouraging information gained from the present experimental results and theoretical discussion could be of practical interest in view of the large implications in the development of polymeric materials for highly add-value applications.

2. Experimental Details

2.1. Materials. Unsupported silicone specimens were supplied by Bluestar Silicones (France) and used as received for the preparation of the silicone rubber membranes. SMs for physical characterization were obtained by mixing the specific RTV-resin silicone casting rubber with the associated catalyst in accordance with the weight ratio specified in Table 1. The obtained materials were placed into a Teflon mould and treated in oven at 353 K for 48 h. Samples with smooth surface were trimmed to a proper size for testing. Before any experiments, the treatment in oven at 353 K was repeated until a constant weight was measured in order to avoid the presence of absorbed moisture. Bulk densities ρ (reported in Table 1) were measured at ambient temperature (average value over three measurements) by using a Micrometrics Accupyc 1300 gas pycnometer under helium atmosphere, having an accuracy of 0.03%.

Wet specimens were prepared by dipping the dry membranes in acetonitrile/methoxypropionitrile solution (AN/MPN; molar ratio 1 : 1) in stopped bottles at room temperature. At regular intervals, the samples were removed from the solvent and repeatedly weighed (electronic balance with an accuracy of ±0.01 mg) until their weight kept constant. A period of 20 ÷ 25 days ensured the achievement of the uptake equilibrium for all the SMs.

The AN/MPN solution was chosen since nitrile based solvents are commonly used as liquid components in DSSCs due to their high solvation activity for the redox couple and rather high boiling temperature. In the sequel of this work, the acronyms SM^{xxx} will be used to designate the studied silicone membranes with the exponent indicating the code of the specific RTV resin silicone casting rubber.

The AN/MPN uptake of the selected membranes was measured as a function of dipping time in the nitrile based solution and calculated as follows:

$$\text{Liquid uptake}\,(\%) = \left(\frac{W_w - W_d}{W_d}\right) \times 100, \tag{1}$$

where W_w and W_d are the weight of the wet and dry samples, respectively (reported in Table 1). The equilibrium liquid uptake was obtained by this equation when no further variations in W_w values were observed.

Furthermore, a rough evaluation of porosity, p, in percentage was obtained by the following equation:

$$\text{porosity}\,(\%) = \left(\frac{W_w - W_d}{\rho_s} \cdot V\right) \times 100, \tag{2}$$

where V is the apparent volume of cylindrical shaped membrane (having a thickness of about 1 mm ± 0.3 and a diameter of 18 mm) and ρ_s (0.8744 gr/cm^3) is the AN/MPN solution density determined by Mohr-Westphal hydrostatic balance. This approximative evaluation of porosity, p, can give a reasonable indication of the empty volume characterizing the specific membrane.

2.2. Methods

2.2.1. Dynamic Mechanical Spectroscopy. The temperature behaviour of the mechanical loss modulus E'' for the dry and wet membranes, in the glass-rubber transition region (123 ÷ 250 K temperature range), was obtained by using a dynamic mechanical analyzer of Triton Technology Ltd., operating in a single cantilever configuration and driven in bending mode at frequencies of 0.3, 3, and 30 Hz with a 2 K/min heating rate. The experimental chamber was kept under a controlled atmosphere of nitrogen during each test. Specimens with a thickness of about 1 mm were trimmed into rectangular shape of approximately 10 mm wide × 30 mm long. The temperature corresponding to the peak in the plot of the loss modulus versus temperature was taken as the glass transition temperature, T_g.

Table 1: Mass density (ρ), dry and wet sample weight, liquid uptake, porosity, and glass transition temperature (T_g) values for the studied membranes.

Samples (abbreviated names)	RTV silicone resin/catalyst (weight ratio)	ρ^a (gr/cm^3)	Sample weight (mgr)		Liquid uptake (%)	Porosity (%)	$T_g{}^b$ (K)
			Dry	Wet			
SM^{689}	96/4	1.48	359.4	360.3	0.25	0.45	148
SM^{Tixo}	95/5	1.21	220.4	222.3	0.86	1.23	147
SM^{400}	95/5	1.19	302.1	324.8	7.50	10.32	143

[a]Determined at room temperature.
[b]Determined on the dry samples at a driving frequency of 3 Hz.

2.2.2. Thermogravimetry and Differential Scanning Calorimetry. Films with a thickness of about 50 μm were prepared for the thermogravimetric analysis by using a film applicator 3570 of Elcometer. TG measurements were carried out on small pieces of sample (10 ÷ 15 mg) at a constant heating rate of 5 K/min in a Setaram thermogravimetric analyzer (SETARAM TG-DSC 111). The thermal stability of dry membranes was determined over a temperature range beyond the working temperature of any DSSCs (293 K ÷ 873 K). TG tests were also performed on wet samples in order to correlate the revealed weight loss with the amount of the liquid electrolyte which escapes from the membrane.

A DSC1-STAR^e System of Mettler-Toledo was used to reveal the existence of crystalline fractions in the polymeric membranes. Dry samples were put inside standard aluminium pan and heated with a rate of 10 K/min in the temperature range from 153 K to 423 K. The magnitude of the features in the thermograms was normalized taking the weights of the samples into account. The melting point of the crystalline phases was taken as the temperature (T_m) corresponding to the maximum of the observed endothermic peak.

2.2.3. SEM and AFM Analyses. SEM was carried out by a field emission scanning electron microscope Phillips XL 30, with an accelerating voltage of 20.0 kV. The image obtained allowed to investigate the surface morphology of SMs down to 20 μm.

The AFM analysis was performed with a Veeco-Innova microscope operating in high amplitude mode. Ultra sharpened Si tips were used (MSNL-10 from Veeco Instruments, with anisotropic geometry, radius of curvature ~2 nm, tip height ~2.5 μm, front angle ~15°, back angle ~25°, and side angle 22.5°) and substituted as soon as a resolution loss was observed during the acquisition. The AFM images were analyzed by using the SPMLabAnalyses V7.00 software and sample roughness, average depth value and depth distribution were obtained. No distortion of the images due to condensation between tip and samples was noted.

3. Results and Discussion

3.1. Dynamic Mechanical Spectroscopy. To illustrate the influence of the AN/MPN mixture on the relaxation dynamics of the studied SMs by crossing the glass transition temperature region, the experimental results for the loss modulus $E''(T)$ at a mechanical frequency of 3 Hz in the dry and wet specimens are compared in the panels of Figure 1. As the temperature is increased from 123 K, $E''(T)$ of both wet and dry samples exhibit a well-defined loss-peak, followed by a large shoulder extending up to about 213 K. Both these features shift to higher temperatures as the driving frequency is increased as a clear indication of the thermally activated nature of the underlying processes (see inset of Figure 1(a), as typical). With increasing temperature above 223 K, a further characteristic, which appears to be frequency independent, is discernible in the $E''(T)$ behaviour for all the specimens. It is worth to point out that the storage modulus $E'(T)$ shows significant inflections in the same temperature region where $E''(T)$ reveals its maxima (not shown here).

With regard to the lower temperature loss-peak, there is a wide agreement that it arises from the primary α_a-relaxation due to the major segmental motions typical of the glass-rubber transition [13–16]. From the curves reported in Figure 1 it appears that the solvent addition to dry membranes has a negligible influence on the α_a-relaxation which keeps almost unchanged its magnitude as well as its peak temperature at a fixed frequency. The only exception is observed for the wet SM^{TIXO} specimen where a slight shift towards lower temperatures together with a weak increase in the peak magnitude is revealed with respect to the dry membrane (see Figure 1(b)). These features could be attributed to a probable weak plasticizing effect [17] of the liquid AN/MPN mixture on the segmental mobility of the polymeric chains.

According to recent mechanical and quasielastic neutron scattering (QENS) measurements [16, 18] detailing with polymer-fillers systems, the second broad relaxation region can be ascribed to the glass-transition of alkyl chains having reduced mobility due to the presence of fillers and/or crystalline regions. Unfortunately, its central temperature cannot be univocally determined due to its unusually large temperature range probably arising from the complex molecular structure of these membranes. In fact, silicone elastomers are always a mixture of different materials (basic polymers, fillers, catalyst, and other additives) chosen to optimize the performances in service. Nevertheless, it is interesting to note that in the SM^{TIXO} and SM^{400} this relaxation region appears to be rather varied going from the dry to wet samples (see Figures 1(b) and 1(c), resp.).

Differently, the almost total invariance observed in the relaxation feature of SM^{689} is a clear indication of no relevant interaction effects between the AN/MPN mixture and

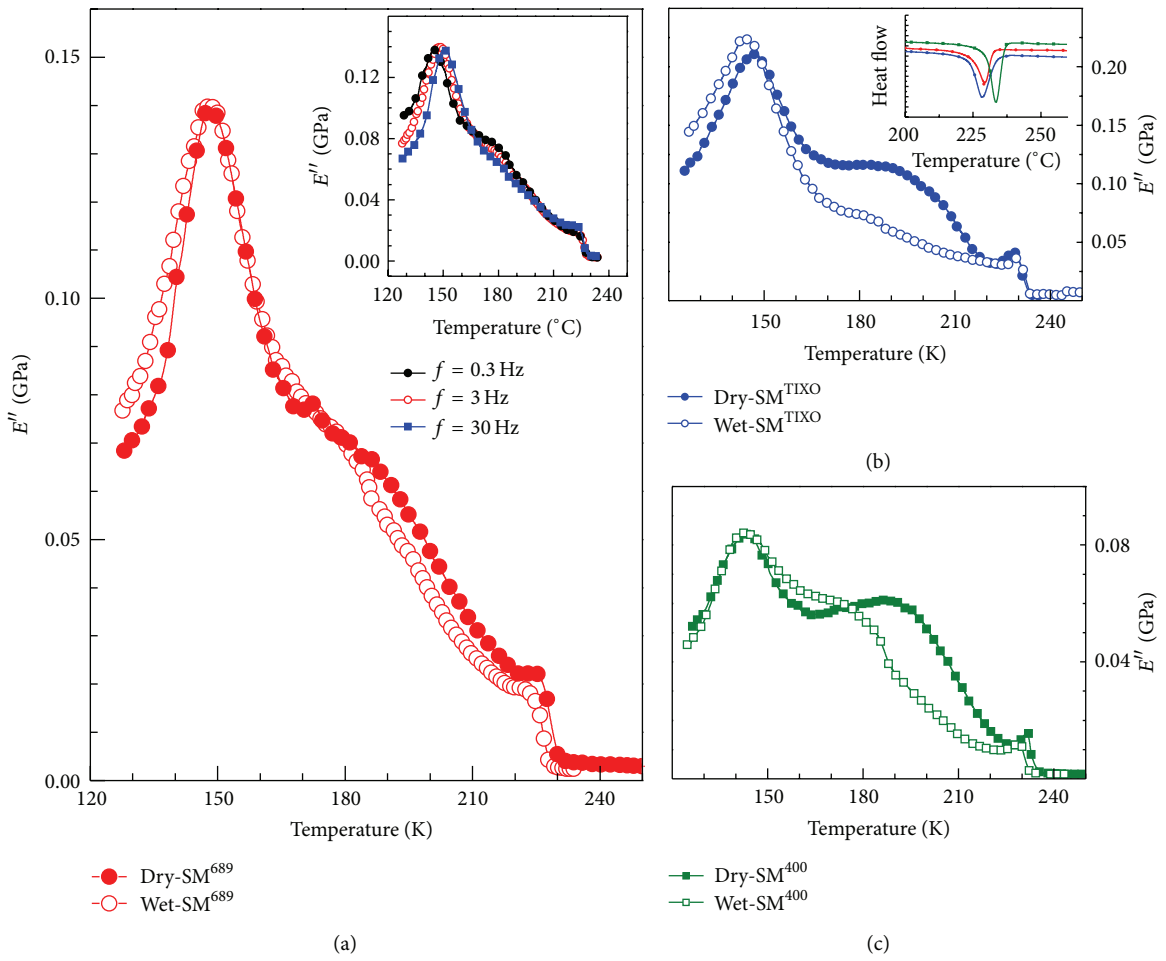

FIGURE 1: Temperature behaviours of the modulus $E''(T)$ in the wet and dry silicone membranes at a driving frequency of 3 Hz for SM^{689} (a), SM^{TIXO} (b), and SM^{400} (c). The inset of panel (a) reports the effect of driving frequency on the temperature dependence of the loss modulus E'' in the wet SM^{689} specimen (as representative). In the inset of panel (b) the DSC traces for all the dry membranes are also shown.

the polymeric matrix, with respect to the other investigated specimens.

Finally, the frequency independence of the third contribution to $E''(T)$, displayed above 213 K, can be considered as an evidence of the semicrystalline nature of the investigated membranes. This hypothesis appears consistent with the DSC results revealing, in this temperature region, a wide endothermic peak (see inset in Figure 1(b)) which is the evidence for the melting of crystalline phases (T_m ranging from about 233 K up to about 228 K).

3.2. Thermal Gravimetric Analysis

3.2.1. Thermal Degradation Stability. The study of thermal stability details the temperature range where the silicone membrane keeps unchanged its specific characteristics without undergoing any degradation processes. This represents a very important piece of information which has to be considered for the use of these materials as liquid confining agents in DSSCs. With this aim, the thermal degradation behaviour of the selected dry membranes was investigated by thermal gravimetric analysis and in Figure 2(a) their weight loss percentages as a function of temperature are reported. With reference to this figure, the superior thermal stability of SM^{689} as compared to the other specimens is immediately apparent. In fact, the weight loss behaviour of this sample is always delayed in temperature with respect to the other membranes. Interestingly, all the samples undergo more than one single degradation step, indicating the probable existence of different degradation mechanisms.

These features can be seen more clearly in the derivative TG curves (DTG) where the weight loss which is observed as a decrement in TG traces is strongly enhanced and revealed as a large peak. More precisely, DTG curves (see Figure 2(b)) show specific features (indicated by arrows for the SM^{TIXO} as example) which are revealed as small shoulders and well-defined peaks. In particular, the feature observed between 488 K and 603 K corresponds to a lower weight loss with respect to that observed at temperature above 603 K which appears particularly enlarged and characterized by a rather complex profile. Owing to its higher magnitude, it can be related to the most relevant degradation process of the

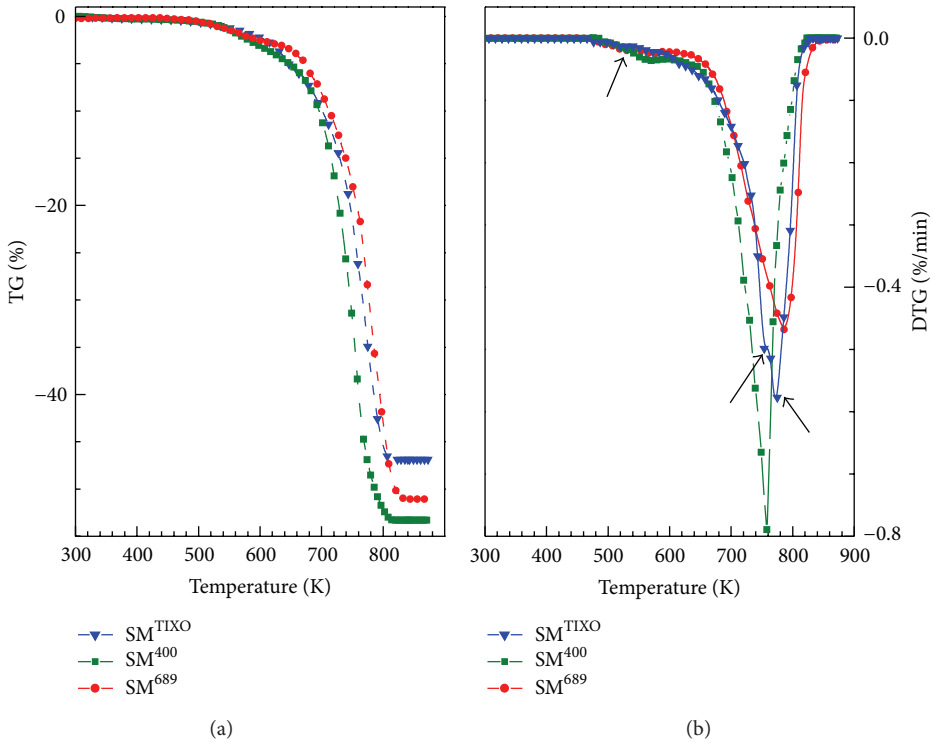

Figure 2: TG (a) and DTG (b) curves of the dry SM^{689} (-•-), SM^{TIXO} (-▼-), and SM^{400} (-■-) samples obtained in nitrogen atmosphere.

membranes. From a qualitative point of view, the temperature interval, ΔT, during which the degradation process occurs, may exhibit a broadening owing to fluctuations of composition on medium/large scale associated with the structural inhomogeneity of these materials. Furthermore, by assuming the peak temperature at its maximum magnitude, T_{max}, as a marker of the thermal degradation of the system, it can be observed that its value shifts from about 758 K in SM^{400}, through ~772 K (SM^{TIXO}), to about 788 K in SM^{689}. Following the experimental results, we suppose that the higher T_{max} in SM^{689} together with its narrow ΔT interval with respect to the other membranes should be related to a higher structural macrohomogeneity which in turn supports a higher thermal stability. Nevertheless, it is worth noting that the weight loss in all the selected membranes starts around 473 K, this temperature being largely higher than the usual working temperature of a DSSC.

3.2.2. Thermal Desorption Behaviour. The liquid uptake data, obtained by (1) and reported in Table 1, give information about the membrane tendency to absorb the AN/MPN liquid solution. In particular, it can be seen that the SM^{689} specimen is characterized by the lowest uptake value as a macroscopic evidence of its smaller affinity towards the liquid mixture. As expected, the data in Table 1 show that, in all the examined samples, the overall liquid uptake and porosity data have opposite trends with respect to density values: the higher the density, the lower the porosity and liquid uptake. Higher densities, in fact, are indicative of a more efficient chain packing which determines a lower porosity and, as a consequence, a decreased liquid uptake. On the other hand, an important requirement for a membrane to efficiently confine the electrolyte solution into a DSSC device is also a low attitude to release the absorbed solvent. In this respect, it is necessary to gain more detailed information on the confinement capability of the membranes. This goal can be obtained by studying the liquid desorption process in wet samples after the uptake equilibrium has been achieved.

Thermogravimetric measurements were performed over the temperature interval between 293 K and 473 K, because no degradation processes were observed in this range. Figure 3(a) shows the temperature dependence of the weight loss for the selected wet membranes, normalized taking into account the total adsorbed liquid amount obtained by liquid uptake data. In this way, the percentage of the absorbed solvent escaping from the bulk materials was determined. As shown in Figure 3(a), the TG curves of the wet membranes have profiles characterized by different slopes corresponding to different weight loss regions. The first one occurs in the 293 ÷ 323 K range and could correspond to the thermodesorption of solvent molecules physically adsorbed on the layers next to the membrane surface. The more consistent second weight loss between 323 ÷ 403 K could be related to solvent molecules which move from the neighboring regions to the outer layers of the membrane. Finally, above 403 K, the weight loss becomes smooth and likely could be ascribed to the residual molecules which have difficulty to escape because coming from the bulky inner region. This last process is supposed to depend on the network structural packing so that it can take place only at higher temperatures when the diffusive process becomes significant.

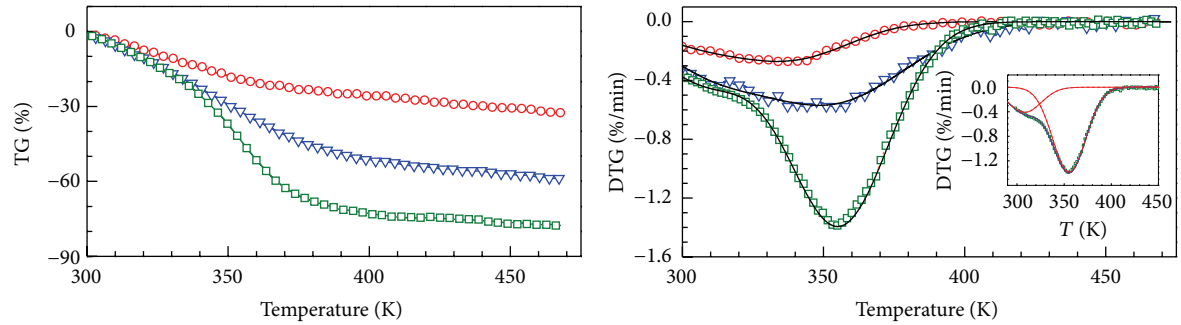

FIGURE 3: TG (a) and DTG (b) curves in the wet silicone membranes: SM^{689} (-○-), SM^{TIXO} (-▽-), and SM^{400} (-□-). The Gaussian fit curves are represented as solid line. In the inset, the experimental DTG curves (open symbol) and the theoretical fit (solid line) together with the two Gaussian peaks (dashed lines) for SM^{400} (as an example) are reported.

TABLE 2: Values of Gaussian fit parameters of the studied wet membranes. The surface roughness and average pore depth obtained by AFM analysis on dry membranes are also reported.

Samples	$T_{p,i}$(K)		FWHH (K)		A_{peak}(%)		Surface roughness (nm)	Average depth (nm)
	$T_{p,1}$	$T_{p,2}$	w_1	w_2	A_1	A_2		
SM^{689}	308	341	313	311	7.5	10.7	0.4	4.5
SM^{Tixo}	308	352	309	325	11.4	36.3	0.5	2.9
SM^{400}	308	355	307	308	14.1	59.0	1.3	3.6

In order to get a more quantitative comparison between the desorption behaviours in the different membranes, the more convincing derivative thermogravimetric curves were also analyzed (see Figure 3(b)).

Interestingly, the peaks of the DTG traces are particularly broad and characterized by an asymmetric shape in the low temperature side. This peculiarity suggests that this feature could derive from the overlapping of two contributions arising from the desorption processes at temperature below 403 K. To separate the two contributions and better quantify the weight loss percentage, a fit of the DTG curves was performed by considering two Gaussian functions. The validity of this approach can be assessed from Figure 3(b), where a comparison between the experimental data (open symbols) and Gaussian fit (solid lines) is also reported.

Table 2 lists the data obtained for both the Gaussian peaks in each membrane: the central peak temperature, $T_{p,i}$, the full width at half height, FWHH, and the peak area, A_{peak}.

The peak temperature and FWHH parameters are related to the maximum rate of weight loss and to how easily the liquid escapes from the bulk material (the narrower FWHH, the easier the desorption process), respectively, while the A_{peak} can be related to the percentage of desorbed solvent. By this analysis, the temperature $T_{p,1}$ of the first Gaussian peak appears invariant for all the SMs. This observation suggests a common origin of the underlying process probably associated to the release of solvent molecules from membrane regions next to the surface. Furthermore its FWHH, w_1, and amplitude, A_1, show opposite trend with increasing porosity according to a reduced time of desorption and a higher amount of desorbed AN/MPN expected from more porous surfaces. Differently, the second Gaussian peak is located at a higher temperature $T_{p,2}$ and is characterized by an amplitude A_2 whose value increases with porosity. In fact, higher temperatures are required to desorb the solvent molecules which move from the inner part of the membrane. Regarding w_2 parameter, it is worth to note that it can be affected by the statistical distributions of pores (different number and/or size) as well as by their tortuosity, τ, which is defined as the ratio of the true length of the flow path and straight-line distance between the beginning and end points [19]. The tortuosity acts as a barrier to the solvent molecules, forcing them to follow longer paths in order to escape away from the bulk material and, as a consequence, the desorption process takes longer time and higher temperatures. In this context, the highest w_2 value shown by SM^{TIXO} could be justified supposing that this membrane is characterized by a more relevant tortuosity of its pores with respect to the other specimens. On the other hand, the similar FWHH values for both Gaussian peaks in SM^{400} could be explained by a homogeneous distribution of small size pores with low tortuosity. As a consequence, the desorption processes from the surface and from the inside of the membrane take place in similar time, but owing to the small dimensions of pores, the second process requires the achievement of a higher internal pressure and a higher temperature.

In order to provide detailed information about the microscopic surface morphology, which affects the membranes performances, SEM and AFM comparative analysis has been carried out. SEM measurements were collected over a selected area of the membrane surface and the two-dimensional images for SM^{400} and SM^{689} are shown in

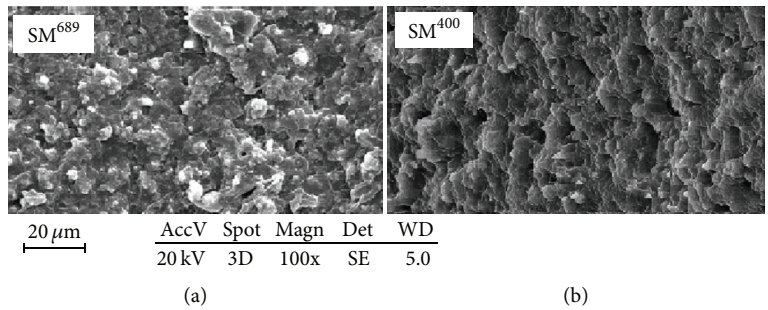

Figure 4: SEM images of the studied SM^{689} (a) and (b) SM^{400} specimens.

Figure 4. It can be seen that the two membranes are characterized by different granulometries, with the SM^{400} specimen showing a more homogeneous distribution of valleys and ridges. Comparatively SM^{689} sample exhibits a more compact surface with an apparent lower roughness which can be correlated with a lower pore distribution. Unfortunately, no direct comparison with SM^{TIXO} was possible, because for this membrane the SEM images were unreliable, probably as a consequence of damaging effects of the electron beam on the membrane surface. Even operating with lower energy electron beam or with greater thicknesses of the membrane no satisfactory SEM images were obtained.

With the aim to better understand the membrane surface morphology, an AFM analysis on all the selected specimens was performed and information about the roughness as well as pore depth distribution of membranes was inferred. Figure 5 shows for each membrane the AFM images in two- and three-dimensional forms over areas of $0.3 \times 0.3\,\mu m$. In the two-dimensional images (see Figure 5(a)), the colour intensity defines the vertical profile of the membranes, where the light and the dark regions refer to the highest and the depression points, respectively. Well-defined dark areas are clearly visible on the images and indicate an increasing number of pores by going from SM^{689} to SM^{400} through to SM^{TIXO}. The analysis of 3D AFM images (see Figure 5(b)) has provided the surface roughness and the pore average depth whose values are reported in Table 2.

By comparing the AFM images of the three membranes, some considerations can be put forward.

(i) The SM^{689} reveals the greatest average pore depth with the narrowest distribution which suggests the existence of pores having a similar size. Furthermore, this membrane shows the lowest roughness reasonably associable with the lowest interface membrane/solvent which, in turn, drives the solvent adsorption/desorption at the surface as well as inside the bulk membrane.

(ii) The SM^{TIXO} shows a 2D image in contrasting heights with a higher density of dark regions with respect to the SM^{689}. By analyzing the 3D image, a surface roughness value similar to that of SM^{689} but with a smaller average pore depth is inferred. These results suggest that this membrane has a greater amount of pores with respect to those observed in SM^{689}.

(iii) The SM^{400} is characterized by the lager dark regions, the highest surface roughness, and the widest pore depth distribution with an average depth value, intermediate between those observed in the other two membranes. These features evidence the existence of a larger number of deeper pores than those revealed in the SM^{TIXO}.

According to Hirose et al. [20, 21] that found a higher liquid permeation with an increasing surface roughness, the lowest solvent sorption/desorption process of SM^{689} can be related to its lowest surface roughness.

It is interesting to observe that all these AFM results well parallel the thermogravimetric data. In fact, with a greater roughness a decreased w_1 and an increased A_1 values are observed because a larger exposed surface implies shorter escape time and larger amount of desorbed solvent. The A_2 parameter shows a similar trend since its value increases with increasing roughness. Finally, SM^{400} and SM^{689} membranes reveal increasing w_2 value with increasing pore depth, in agreement with expected longer realising time for the solvent escaping from inner regions. In this contest, though SM^{TIXO} is characterized by the lowest average depth of pores, its higher w_2 value could be ascribed to a higher pore tortuosity which would imply longer desorption time.

The mechanical, calorimetric, thermogravimetric, SEMs and AFM experimental results show that these membranes are characterized by a low level of liquid uptake and desorption, putting forward their promising employment as sealant for the liquid solution inside DSSC. In this study, the SM^{689} membrane, whose mechanical behaviour is not affected by the solvent presence, emerges as the most suitable membrane for this specific application since it is characterized by the lowest roughness and porosity which imply a poor liquid uptake and desorption.

4. Conclusion

A study of the absorption-desorption process in a set of RTV-silicone membranes has been performed to explore their possible application as sealing materials for liquid solutions which are essential for high electrochemical performances

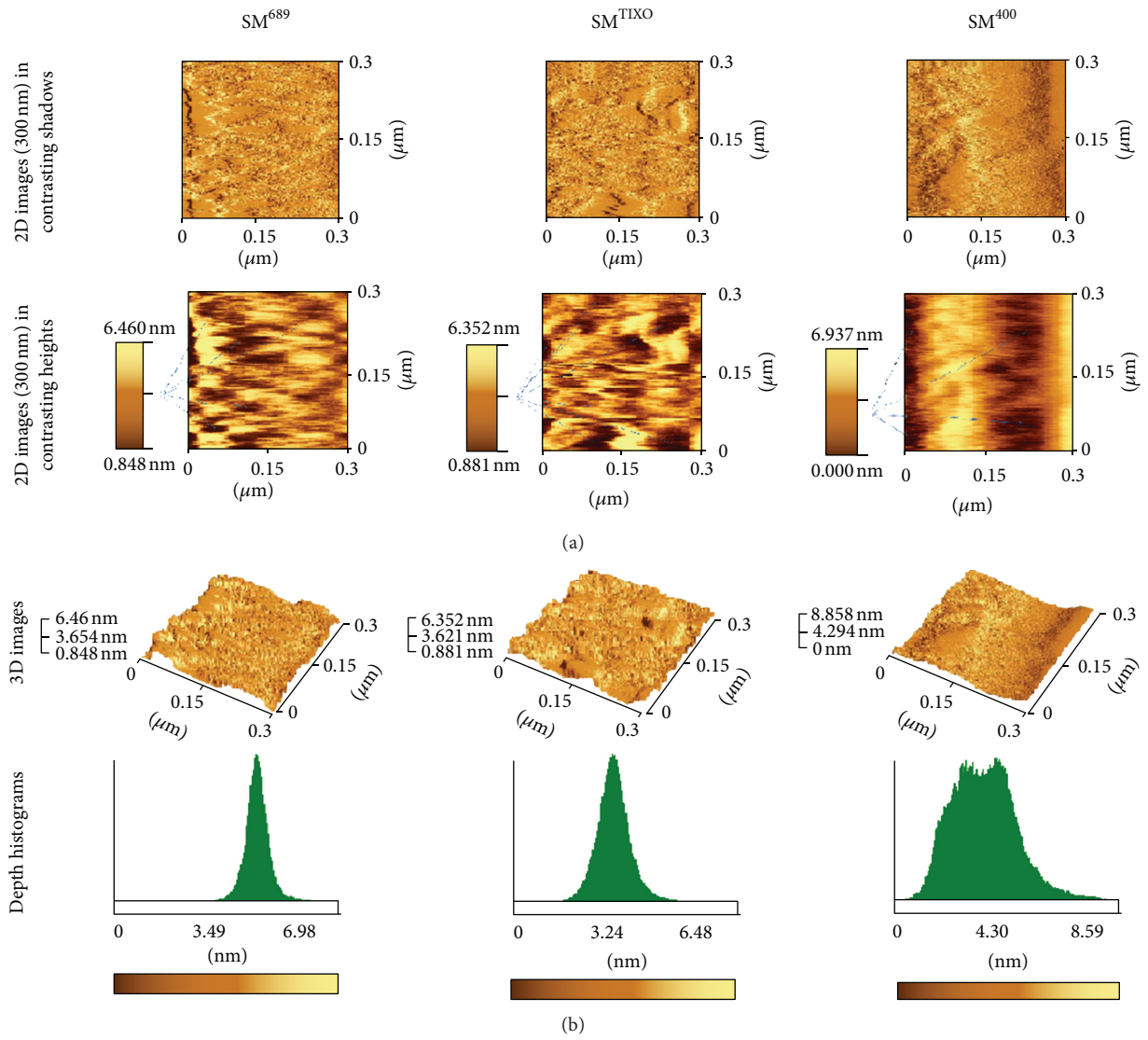

Figure 5: AFM images of the studied membranes: (a) 2D images in contrasting shadows and heights; (b) 3D images and depth histograms.

of a DSSC. Thermo-gravimetric analysis has been applied to evaluate the liquid confining properties of membranes fully saturated by solvent, revealing that the absorption-desorption process is mainly driven by the pore distribution at the surface and inside the bulk membrane. SEM and AFM analysis has disclosed superficial pore distributions which are in agreement with porosity and uptake data, justifying the observed absorption-desorption behaviour. The totality of the experimental results indicate the membrane SM^{689} as the best choice for the discussed application because it maximizes a high thermal stability with a low aptitude to absorb-desorb the AN/MPN mixture over the operating temperature range of DSSC.

This work, combining thermogravimetric measurements, liquid uptake data, and microscopic surface morphology analysis, represents an initial framework to find appropriate materials which could lead to overcome the problem regarding the leakage of volatile liquid components in DSSCs.

Conflict of Interests

None of the authors have a direct financial relation with the trademarks mentioned in this paper that might lead to a conflict of interests for any of them.

Acknowledgments

The authors are grateful to Dr. R. Pedicini (ITAE-CNR, Messina) and to Dr. F. Ruffino (Physical Department, University of Catania) for their collaboration concerning the SEM and AFM measurements, respectively. This research was supported by "EFOR" Project (Energia da FOnti Rinnovabili, Iniziativa CNR per il Mezzogiorno L. 191/2009 art. 2 comma 44) and by "SAGRO" Project financed by Regione Siciliana (Assessorato Regionale Attività Produttive progetti PO FESR 2007/2013 linea d'intervento 4.1.1.1). Furthermore, the authors acknowledge Programma Operativo Nazionale Ricerca e Competitività 2007–2013—project PON 01_02257 FOTORIDUCO2.

References

[1] M. Grätzel and B. O'Regan, "A low-cost, high-efficiency solar cell based on dye-sensitized colloidal TiO_2 films," *Nature*, vol. 353, pp. 737–740, 1991.

[2] M. Grätzel, "Conversion of sunlight to electric power by nanocrystalline dye-sensitized solar cells," *Journal of Photochemistry and Photobiology A*, vol. 164, no. 1–3, pp. 3–14, 2004.

[3] P. V. Kamat, "Meeting the clean energy demand: nanostructure architectures for solar energy conversion," *Journal of Physical Chemistry C*, vol. 111, no. 7, pp. 2834–2860, 2007.

[4] A. Hagfeldt, G. Boschloo, L. Sun, L. Kloo, and H. Pettersson, "Dye-sensitized solar cells," *Chemical Reviews*, vol. 110, no. 11, pp. 6595–6663, 2010.

[5] G. Calogero and G. di Marco, "Red Sicilian orange and purple eggplant fruits as natural sensitizers for dye-sensitized solar cells," *Solar Energy Materials & Solar Cells*, vol. 92, no. 11, pp. 1341–1346, 2008.

[6] G. Calogero, J.-H. Yum, A. Sinopoli, G. di Marco, M. Grätzel, and M. K. Nazeeruddin, "Anthocyanins and betalains as light-harvesting pigments for dye-sensitized solar cells," *Solar Energy*, vol. 86, no. 5, pp. 1563–1575, 2012.

[7] U. Bach, D. Lupo, P. Comte et al., "Solid-state dye-sensitized mesoporous TiO_2 solar cells with high photon-to-electron conversion efficiencies," *Nature*, vol. 395, no. 6702, pp. 583–585, 1998.

[8] J. Wu, S. Hao, Z. Lan et al., "A thermoplastic gel electrolyte for stable quasi-solid-state dye-sensitized solar cells," *Advanced Functional Materials*, vol. 17, no. 15, pp. 2645–2652, 2007.

[9] A. Hinsch, J. M. Kroon, R. Kern et al., "Long-term stability of dye-sensitised solar cells," *Progress in Photovoltaics*, vol. 9, no. 6, pp. 425–438, 2001.

[10] R. Sastrawan, J. Beier, U. Belledin et al., "New interdigital design for large area dye solar modules using a lead-free glass frit sealing," *Progress in Photovoltaics*, vol. 14, no. 8, pp. 697–709, 2006.

[11] W. Noll, *Chemistry and Technology of Silicones*, Academic Press, New York, NY, USA, 2nd edition, 1968.

[12] A. Ghosh and S. K. De, "Dependence of physical properties and processing behavior of blends of silicone rubber and fluororubber on blend morphology," *Rubber Chemistry and Technology*, vol. 77, no. 5, pp. 856–872, 2004.

[13] J. C. Lötters, W. Olthuis, P. H. Veltink, and P. Bergveld, "The mechanical properties of the rubber elastic polymer polydimethylsiloxane for sensor applications," *Journal of Micromechanics and Microengineering*, vol. 7, no. 3, pp. 145–147, 1997.

[14] H.-T. Chiu, S.-H. Chiu, and J.-H. Wu, "Study on mechanical properties and intermolecular interaction of silicone rubber/polyurethane/epoxy blends," *Journal of Applied Polymer Science*, vol. 89, no. 4, pp. 959–970, 2003.

[15] A. Ghosh, A. K. Naskar, D. Khastgir, and S. K. De, "Dielectric properties of blends of silicone rubber and tetraflouroethylene/propylene/vinylidene fluoride terpolymer," *Polymer*, vol. 42, no. 24, pp. 9849–9853, 2001.

[16] V. Arrighi, J. S. Higgins, A. N. Burgess, and G. Floudas, "Local dynamics of poly(dimethyl siloxane) in the presence of reinforcing filler particles," *Polymer*, vol. 39, no. 25, pp. 6369–6376, 1998.

[17] P. C. Painter and M. M. Coleman, *Essentials of Polymer Science and Engineering*, DEStech Publications, Lancaster, Pa, USA, 2009.

[18] G. Tsagaropoulos and A. Eisenberg, "Dynamic mechanical study of the factors affecting the two glass transition behavior of filled polymers. Similarities and differences with random ionomers," *Macromolecules*, vol. 28, no. 18, pp. 6067–6077, 1995.

[19] M. Sahimi, *Flow and Transport in Porous Media and Fractured Rock*, Wiley-VCH, 2nd edition, 1995.

[20] M. Hirose, H. Itoh, and Y. Minamizaki, "Ultra-low-pressure reverse osmosis membranes ES 10," in *Proceedings of the International Congress on Membranes and Membrane Process*, pp. 178–179, Yokohama, Japan, August 1996.

[21] M. Hirose, H. Ito, and Y. Kamiyama, "Effect of skin layer surface structures on the flux behaviour of RO membranes," *Journal of Membrane Science*, vol. 121, no. 2, pp. 209–215, 1996.